

Numerical Investigation on Flow and Heat Transfer Performance of Supercritical Carbon Dioxide Based on Variable Turbulent Prandtl number Model

Xiaokai LIU^{1,2,3}, Haiyan ZHANG^{1,2}, Keyong CHENG^{1,2,3*}, Xiulan HUAI^{1,2,3*}, Haiyan LIAO⁴, Zhongmei ZHANG⁴

1. Institute of Engineering Thermophysics, Chinese Academy of Sciences, Beijing 100190, China
2. University of Chinese Academy of Sciences, Beijing 100049, China
3. Nanjing Institute of Future Energy System, Nanjing 210000, China
4. CHN Energy New Energy Technology Research Institute CO., LTD., Beijing 102206, China

*Corresponding Author: Keyong CHENG, E-mail: chengkeyong@iet.cn, Xiulan HUAI, hxl@iet.cn

Abstract:

Flow and heat transfer characteristic of supercritical carbon dioxide (SCO₂) are numerically investigated in the horizontal and vertical tubes. TWL turbulent Prandtl number model could well describe the behavior of SCO₂ affected by the buoyancy. Under the cooling condition, the heat transfer performance of SCO₂ along the upward direction is best and that along the downward direction is worst when bulk fluid temperatures are below the pseudocritical temperature. Reducing the ratio of heat flux to mass flux could decrease the difference of convective heat transfer coefficient in three flow directions. Under the heating condition, heat transfer deterioration only occurs in vertical upward and horizontal flow directions. Heat transfer deterioration of SCO₂ could be delayed by increasing the mass flux and the deterioration degree is weakened in the second half of tube along the vertical upward flow direction. Compared with the straight tube, the corrugated tube shows better comprehensive thermal performance.

Keywords: Supercritical carbon dioxide; Turbulent Prandtl number; Flow and heat transfer; Field synergy principle; Numerical investigation

Table 1 Nomenclature

| c_p | Specific heat at constant pressure, J/(kg K) |
|------------|--|
| d | Diameter, mm |
| g | Gravity, m/s ² |
| G | Mass flux, kg/(m s) |
| h | Heat transfer coefficient, kw/(m K) |
| P | Pressure, mpa |
| q | Heat flux, kw/m |
| Re | Reynolds number |
| T | Temperature, K |
| T_{pc} | Pseudocritical temperature, K |
| v | Velocity, m/s |
| Greek | |
| λ | Thermal conductivity, W/(m K) |
| μ | Dynamic viscosity, Pa s |
| ρ | Density, kg/m ³ |
| τ | Shear stress, Pa |
| ϕ | Energy dissipation, W/m ³ |
| Subscripts | |
| ave | Average |
| b | Bulk |
| i, j, k | Tensor index symbols |
| w | Wall |

1 Introduction

Carbon dioxide (CO₂) is widely used in advanced energy power systems due to its excellent characteristics of wide sources, non-toxic and environmental protection. Since the supercritical CO₂ (SCO₂) Brayton cycle system can significantly reduce system size, improve system efficiency and decrease investment cost, the SCO₂ power generation technology has attracted wide attentions^[1-3]. Under supercritical pressure, the thermophysical properties of SCO₂ are changed dramatically around the pseudocritical point (the peak point of specific heat at constant pressure corresponds to the pseudocritical temperature (T_{pc}), which is called pseudocritical point.), which would induce the various heat transfer behavior. Therefore, it is very important to further explore flow and heat transfer behaviors of SCO₂ under supercritical pressure.

In recent years, many researchers have studied flow and heat transfer characteristics of SCO₂ by numerical and experimental methods. Liu et al.^[4] studied the Nusselt number and pressure loss of SCO₂ in a large diameter tube through the experiments, and they

summarized the empirical correlation. Jiang et al. [5] conducted experiment study on the effects of flow direction, heat flux and buoyancy effect. Xu et al. [6] studied the thermal performance of SCO₂ in serpentine tubes. The buoyancy and centrifugal force in different flow directions were investigated. Zhu et al. [7] obtained the criterion of heat transfer deterioration by experiments. Liu et al. [8] introduced the influence of buoyancy effect and centrifugal force on SCO₂ in helical tubes.

Due to only limited temperature data can be obtained from the experiment, the flow field in the tube cannot be analyzed in detail. To understand the heat transfer mechanism of SCO₂, numerical methods have been widely used. Liu et al. [9-10] numerically studied the effects of pipe cross-section shapes and diameters on SCO₂. They found that the pipe shape and pipe diameter have great influence on the secondary flow strength of SCO₂. The performance of SCO₂ in straight and helical tubes is compared by Liu et al. [11]. They stated that the centrifugal force could make the heat transfer capacity of the spiral tube stronger than that of the straight tube, but the centrifugal force in the pseudocritical region can cause more serious deterioration. Eze et al. [12] found that the heat transfer deterioration of SCO₂ could be effectively reduced by adding spoilers in the pipe. The effects of heat and mass flux on the comprehensive mechanism of SCO₂ are explored by Yan et al. [13].

In this study, flow and heat transfer of SCO₂ in straight and corrugated tubes are presented. During the simulations, different mass flux, heat flux, and flow direction are analyzed and discussed. This research may be helpful for the understanding of SCO₂ heat transfer.

2 Numerical Model

2.1 Physical model and simulation conditions

The physical models of straight and corrugated tubes are established in the present work and the orthographic view of the geometry model is shown in Figure 1. The heated length of two tubes is set to 900 mm. The tube diameter is 6 mm, and the adiabatic sections are arranged at the inlet and outlet of the tube respectively. The inlet pressure is fixed to 8 MPa.

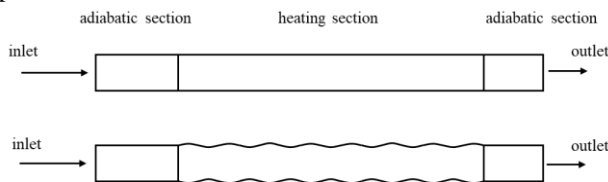


Figure 1 Physical model and simulation conditions

2.2 Governing equations

The software ANSYS FLUENT 19.2 is employed for the calculations. The steady-state equations are listed in Eq. (1)-(3):

Continuity equation:

$$\frac{\partial(\rho u_j)}{\partial x_j} = 0 \quad (1)$$

Momentum equation:

$$\frac{\partial(\rho u_i u_j)}{\partial x_j} = -\frac{\partial P_i}{\partial x_j} + \rho g_i + \frac{\partial}{\partial x_j} \left[(\mu + \mu_t) \left(\frac{\partial u_i}{\partial x_j} + \frac{\partial u_j}{\partial x_i} - \frac{2}{3} \frac{\partial u_k}{\partial x_k} \right) \right] \quad (2)$$

Energy equation:

$$\frac{\partial(\rho u_j c_p T)}{\partial x_j} = \frac{\partial}{\partial x_j} \left(\lambda \frac{\partial T}{\partial x_j} \right) + \phi \quad (3)$$

The Shear Stress Transport (SST) model is employed in the present work, which has been proved accurately to calculate the heat transfer behavior of SCO₂ [14-15]. The equations of the turbulence kinetic energy k and the specific dissipation rate ω are listed in Eq. (4) and (5), respectively:

$$\frac{\partial(\rho k)}{\partial t} + \frac{\partial(\rho k u_i)}{\partial x_i} = -\frac{\partial}{\partial x_j} \left(\Gamma_k \frac{\partial k}{\partial x_j} \right) + G_k - Y_k + S_k \quad (4)$$

$$\frac{\partial(\rho \omega)}{\partial t} + \frac{\partial(\rho \omega u_i)}{\partial x_i} = -\frac{\partial}{\partial x_j} \left(\Gamma_\omega \frac{\partial \omega}{\partial x_j} \right) + G_\omega - Y_\omega + S_\omega \quad (5)$$

2.3 Turbulent Prandtl number model

The Pr_t is set to 0.85 or 0.9, which is obtained at atmospheric pressure and it is not applicable to supercritical fluids with severe physical changes. Li et al. [16] claimed that the turbulence kinetic energy of the buffer layer decreased for the deterioration and the appropriate Pr_t model is crucial to describe the heat transfer characteristics of SCO₂.

In 1993, Kays and Crawford [17] launched the KC model of turbulent Prandtl number as shown in Eq. 6.

$$Pr_t = \begin{cases} 1.07, & y^+ \leq 5 \\ \frac{1}{0.5882 + 0.228 \frac{\mu_t}{\mu} - 0.0441 \left(\frac{\mu_t}{\mu} \right)^2 \left[1 - \exp \left(-\frac{5.165}{\mu_t/\mu} \right) \right]}, & y^+ > 5 \end{cases} \quad (6)$$

Kays proposed the K model in 1994, and this turbulent Prandtl number model agrees well with the experiment of Buhret al [18].

$$Pr_t = \begin{cases} 1.07, & y^+ \leq 5 \\ 0.85 + \frac{2}{Pe_t}, & y^+ > 5 \end{cases} \quad (7)$$

Where $Pe_t = \mu_t / \mu Pr$.

For the flow of SCO₂ under high Reynolds number conditions, the turbulence is a key parameter. Therefore, Pr_t tends to be constant. In the viscous bottom, the Pr_t effect is limited due to the leading role of the molecular heat conduction. However, u and u_t are in the same magnitude order for the transition region. Tang et al. [19] proposed TWL model of turbulent Prandtl number as shown in Equation 8.

$$Pr_t = \begin{cases} 1.0, & \mu_t / \mu < 0.2 \\ 0.85 + \frac{Pr}{15}, & 0.2 \leq \mu_t / \mu \leq 10 \\ Pr = 10, & \mu_t / \mu > 10 \end{cases} \quad (8)$$

2.4 Grid number independence and model validation

Considering the influence of grid number on the calculation results, four groups of grid numbers generated by ANSYS ICEM 19.2 are selected for grid independent verification. The grid numbers and calculation results are shown in Table 2. The maximum relative error of the h between Case 3 and Case 4 is only about 2.8%. Take into account both calculation accuracy and cost, grid number in Case 3 is selected for the calculation in following calculations.

Table 2 The grid number independence test

| Case | Grid number | h (kW/(m ² K)) | Relative error |
|------|-------------|-----------------------------|----------------|
| 1 | 695656 | 1.077 | 9.7% |
| 2 | 1226960 | 1.019 | 3.8% |
| 3 | 1576248 | 1.009 | 2.8% |
| 4 | 2113160 | 0.982 | - |

The reliability of simulation is further verified by establishing the same physical model and setting the same boundary conditions in Ref. [20]. Three Pr_t models introduced in section 2.3 are selected for numerical calculation, and the corresponding wall temperature distribution is presented in Figure 2. The maximum relative error of T_w between simulation and experiment is about 4 %, which illustrates that the SST turbulence model and TWL Prandtl number model is accurate and credible to simulate flow and heat transfer of SCO₂.

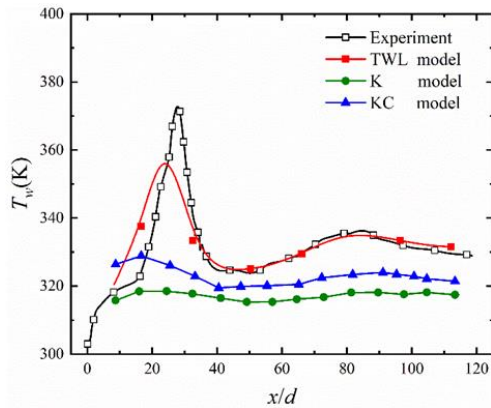


Figure 2 Comparison of turbulent Prandtl number models under experiment conditions

3 Results and Discussion

3.1 Cooling conditions in straight tubes

Figure 3 shows that for the cooling conditions the effect of the heat flux to mass flux ratio q/G on the wall temperature of the tube T_w . It can be found that the T_w decreases with the decrease of T_b . When the G is fixed, the T_w decreases with the enlargement of q , and the T_w increases with the raise of G When the q is fixed. Therefore, the T_w decreases with the increase of q/G , and the range of fluid temperatures increases with the enlargement of q/G . At $G = 200 \text{ kg}/(\text{m}^2 \text{ s})$, when the fluid

bulk temperature is slightly higher than the pseudocritical temperature (307.8 K at 8 MPa), it can be found that T_w upward $> T_w$ horizon $> T_w$ downward. In the region where the T_b is larger than T_{pc} , the distribution of T_w tends to be consistent in horizontal, vertical upward and vertical downward directions. There is almost no difference in the distributions of T_w with three flow directions when the mass flux is $500 \text{ kg}/(\text{m}^2 \text{ s})$.

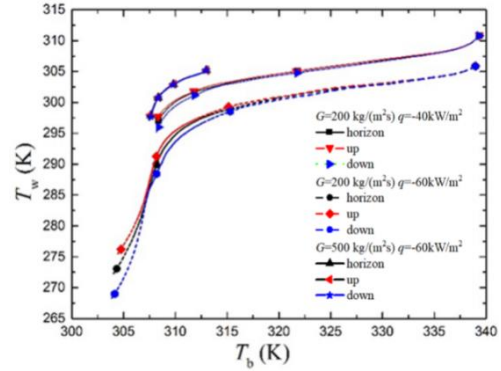


Figure 3 Variation of wall temperature with fluid temperature

The influence of buoyancy is considered because of the drastic changes of the density of SCO₂. The buoyancy factor Gr/Re^2 is employed to describe buoyancy effects in the horizontal flow direction and the expression of Grashof number Gr is shown in equation 9. Generally, the natural convection induced by buoyancy remarkably affects the thermal-hydraulic characteristics for $Gr/Re^2 > 0.001$. The effect of natural and forced convection on heat transfer is necessary to be considered simultaneously for $0.1 < Gr/Re^2 < 10$. When $Gr/Re^2 > 10$, compared with natural convection, forced convection can be ignored. The buoyancy factor $Gr/Re^{2.7}$ is adopted to characterize the buoyancy effect of the vertical upward and downward flow. It is generally accepted that the influence of the buoyancy force cannot be ignored for $Gr/Re^{2.7} > 10^{-5}$.

$$Gr^* = \frac{g\beta qd^4}{\lambda_b v_b^2} \quad (9)$$

Where β is the fluid volume expansion coefficient.

The variations of h and Gr/Re^2 with T_b are shown in Figure 4 (a) and (b). The h under various conditions first increases and then decreases, and there is a peak at slightly higher temperature than the pseudocritical point. With the increase of the q , the h is enhanced in the region where T_b is much higher than T_{pc} , but there is no effect of the peak value of h . As the T_b decreases to the T_{pc} , it can be seen that $h_{\text{upward}} > h_{\text{horizon}} > h_{\text{downward}}$, but when the mass flow rate is $500 \text{ kg}/(\text{m}^2 \text{ s})$, the heat transfer coefficients for the three flow directions are almost the same, which are consistent with the distribution of T_w presented in Figure 3.

With the increase of q/G , the buoyancy effect is increased at three flow directions, and the effect of buoyancy could be basically ignored when the mass flux is $500 \text{ kg}/(\text{m}^2 \text{ s})$. When the mass flux is $200 \text{ kg}/(\text{m}^2 \text{ s})$, the

buoyancy factor gradually increases with the cooling of the SCO₂, and rapidly increases to the peak near the pseudocritical point which indicates that the buoyancy near the pseudocritical region is strong under the cooling condition. The buoyancy factor of the vertical downward flow is larger compared with upward flow. Combined with the results that $h_{\text{upward}} > h_{\text{downward}}$ from Figure 4 (a), it can be concluded that under the same q/G cooling condition, compared with the vertical downward flow, the vertical upward flow has less buoyancy effect and presents better thermal performance.

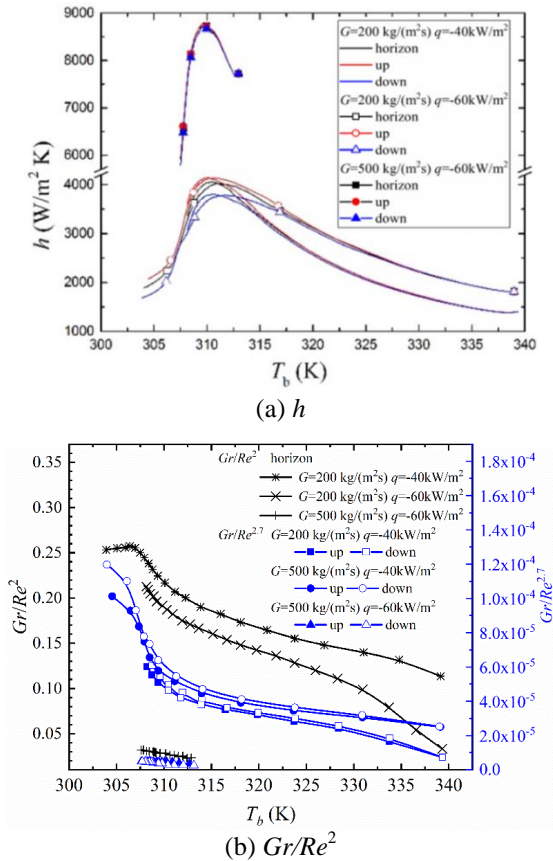


Figure 4 Variation of (a) local heat transfer coefficient and (b) buoyancy factor with fluid temperature.

3.2 Heating conditions in straight tubes

Figure 5 demonstrates the variations of the T_w with the T_b along the horizontal and vertical flow directions. For a horizontal flow, when the mass flux is set to 500 kg/(m² s), T_w increases monotonically. There are wall temperature peaks when the mass flux is set to 200 kg/(m² s). It is seen that there are wall temperature peaks in upward flow direction under the three conditions in Figure 5(b), and when q is fixed, the peak of T_w becomes more obvious with the increases of q . When q/G is small, the peak value of T_w also appears, and the wall temperature variation trends different from the other two heating conditions, and this phenomenon will be further discussed in the subsequent work. The wall temperature monotonically increases, and there is no obvious peak at

the vertical downward flow direction shown in Figure 5(c).

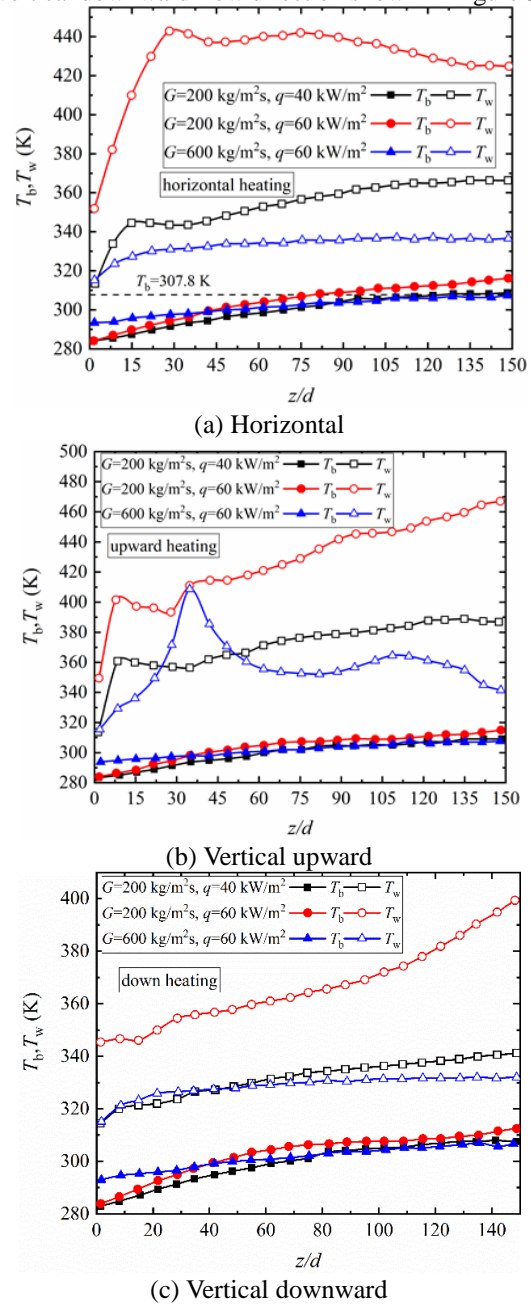


Figure 5 Variations of T_w with T_b under heating conditions: (a) horizontal (b) vertical upward

The variations of h with the T_b at horizontal and vertical flow directions are presented in Figure 6. Figure 6(a) and (c) show that h increases as G grows at the same heat flux, and h decreases as q increases when G is fixed. h shows a decreasing trend from the initial region of the heating section, which is due to T_w increases rapidly along the heating process, resulting in the rapid increase of the temperature difference between the fluid and the wall. Different from the horizontal and vertical downward flow, Figure 6(b) demonstrates that h appears a valley near the region of $z = 35 d$ when the mass flux is 500 kg/(m² s), which means the heat transfer is deteriorated, this phenomenon corresponds to the peak of wall

temperature at about $z = 35 d$. In summary, the enlargement of the q induces the rapid increase of T_w , resulting in the decrease of h under small mass flux condition. When q is 60 kW/m^2 , heat transfer deterioration occurs at mass flux of 200 and $500 \text{ kg/(m}^2 \text{ s)}$, but the increase of G delays the occurrence of heat transfer deterioration and attenuates the degree of deterioration in the second half of heating tube. Thus, it is meaningful to explore the onset and mechanism of heat transfer deterioration under upward flow heating conditions.

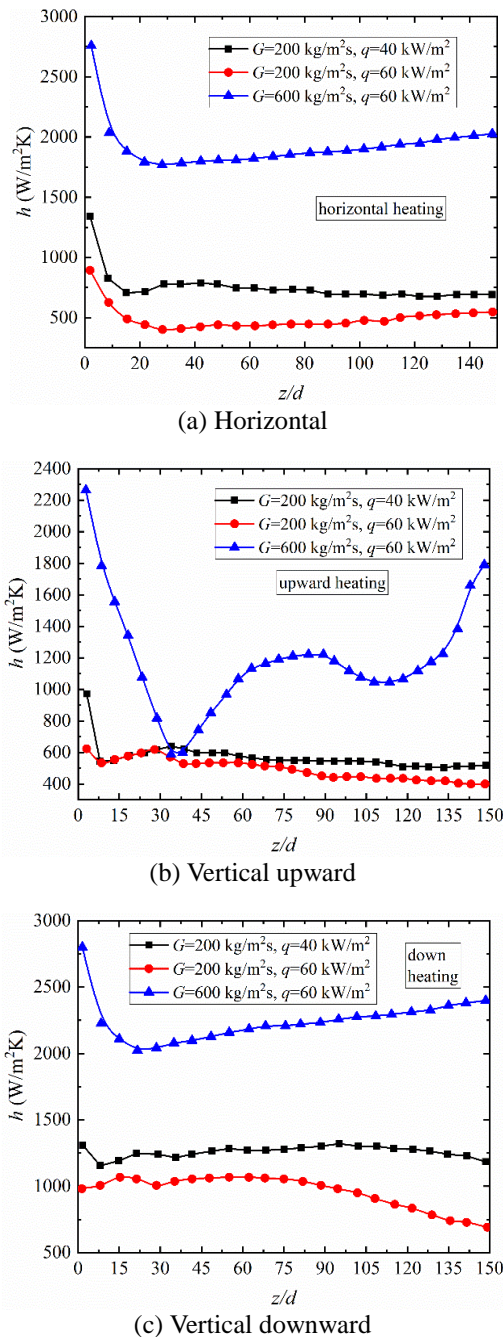


Figure 6 Variations of h with T_b under heating conditions: (a) horizontal (b) vertical upward (c) vertical downward

The relations of buoyancy factor with the bulk fluid temperature at different flow directions are demonstrated in

Figure 7. Figure 7(a) illustrates Gr/Re^2 generally decreases as the T_b increases, and the influence of buoyancy on horizontal flow is the smallest at $G = 500 \text{ kg/(m}^2 \text{ s)}$. It is seen that the buoyancy effect of the vertical upward flow is greater than that of the vertical downward flow.

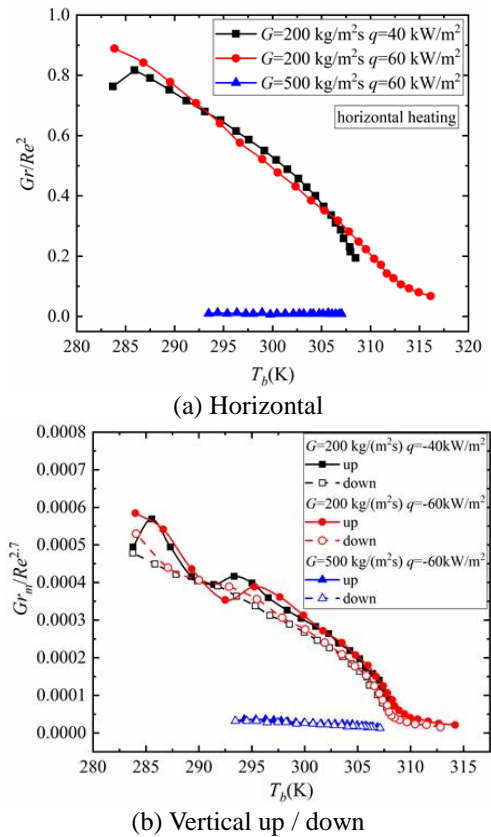


Figure 7 Variations of buoyancy factor with T_b under heating conditions: (a) horizontal (b) vertical up/down.

3.3 Corrugated tubes

The distribution of the T_b and the T_w in corrugated and straight tubes along the horizontal direction is presented in Figure 8. T_b in corrugated and straight tubes is basically the same with the same q and G . However, the wall temperature in corrugated tube fluctuates along the flow direction and T_w is generally higher than that in the straight pipe.

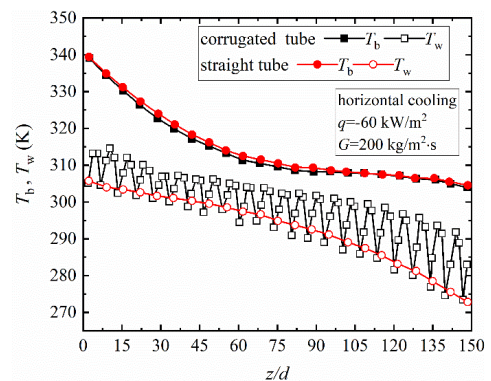


Figure 8 Distribution of bulk fluid temperature T_b and wall temperature T_w in corrugated and straight tubes

The distributions of h and the local evaluation factor $j/f^{1/3}$ in corrugated and straight tubes are provided in Figure. 9. h of a corrugated tube is significantly higher than that of a straight tube. Considering that the corrugated tube usually increases the pressure drop remarkably while enhancing the heat transfer, the evaluation factor $j/f^{1/3}$ is adopted to assess the comprehensive property of the straight and corrugated tubes. It could be concluded that the comprehensive thermal performance of SCO_2 in a corrugated tube is better than that in a straight tube from Figure. 9(b).

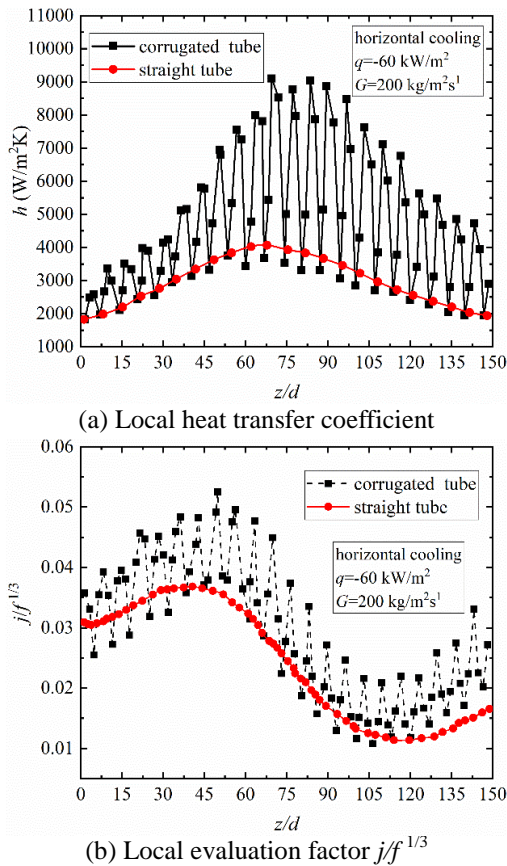


Figure 9 Distributions of local heat transfer coefficient and local evaluation factor $j/f^{1/3}$ in corrugated and straight tubes

Figure 10 and 11 illustrate the distributions of the secondary flow and field synergy angle β on different locations of the corrugated and straight tube under the horizontal cooling condition. The secondary flow in the straight pipe is uniformly distributed, and the left and right vortices are vertically axisymmetric. The velocity of the secondary flow in the corrugated tube is larger than that in the straight tube, and the distribution of the secondary flow is non-uniform. There are multiple asymmetrically distributed vortices and the location of the vortices is complex and variable at different cross sections. In the straight tube, the smaller β is mainly concentrated in the upper of the cross section, but the overall β is almost 90° . In the corrugated tube, the distribution of the field synergy angle on the cross section is non-uniform, and the overall β is smaller than that in the straight tube. According to the field synergy theory, due to the high intensity and uneven distribution of the

secondary flow, the fluid in the corrugated tube is more fully mixed, which enhances the synergy between the local fluid velocity and temperature gradient.

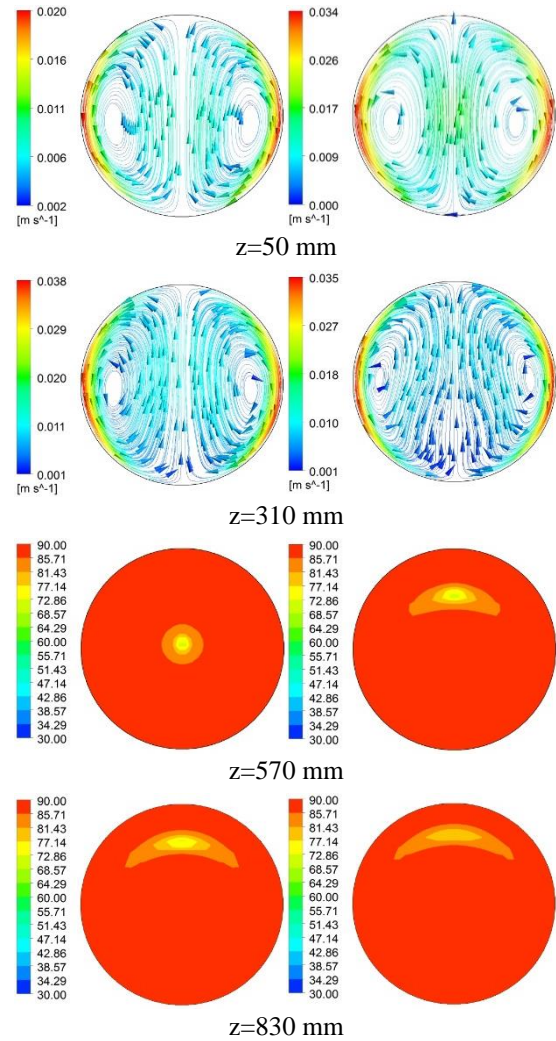
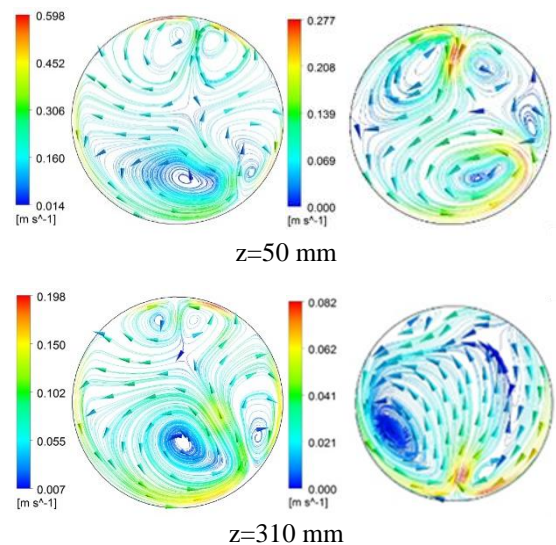


Figure 10 Field synergy angle distribution of the secondary flow and field on the local section of the straight tube



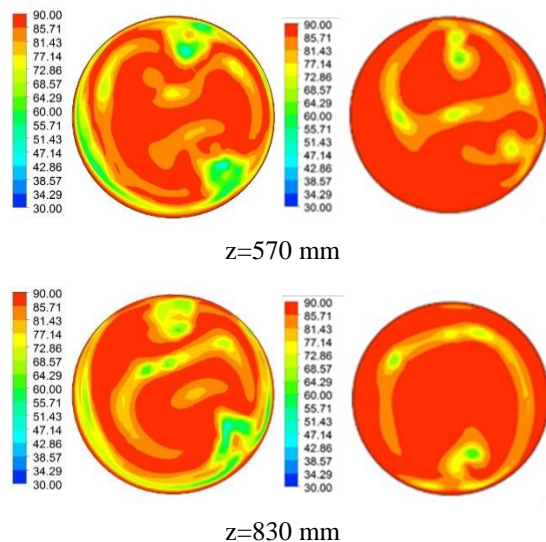


Figure 11 Field synergy angle distribution of the secondary flow and field on the local section of the corrugated tube

4 Conclusions

The flow and heat transfer characteristics of SCO_2 in straight and corrugated tubes are numerically studied. The effects of mass flux, heat flux, flow direction and buoyancy on the heat transfer performance of SCO_2 are analyzed and discussed. The conclusions are listed as follows:

The selected SST $k-\omega$ turbulence model and different turbulence Prandtl number models could reproduce the difference of the wall temperature distribution caused by buoyancy in the experiment, but the TWL Prandtl number model has the best consistency with the experiment data, which could more accurately describe the effect of buoyancy. It is suggested that this model be applied to numerical simulation of thermal-hydraulic characteristics of SCO_2 .

Under the cooling condition in the straight tube, the T_w monotonically decreases along the flow direction, and there is no peak of T_w in the vertical upward, vertical downward and horizontal flow directions. The h peaked near the pseudocritical point. The buoyancy factor in the vertical downward flow is larger than that in the upward flow at the vicinity of pseudocritical point under the cooling condition. As the fluid temperature decreases to less than the pseudocritical temperature, $h_{\text{upward}} > h_{\text{horizontal}} > h_{\text{downward}}$. But, when q/G is small, there is almost no difference on h for the three flow directions.

Under the heating condition in the straight tube, the peak of the T_w only appears in the conditions of the upward and horizontal flow, and there is no wall temperature peak in the vertical downward flow. The increase of the q leads to the rapid enlargement of the T_w , resulting in the decrease of the h with the same G in the vertical upward flow. When the q is fixed, the increase of the G delays the occurrence of heat transfer deterioration and attenuates the deterioration degree in the vertical

upward flow direction.

The comprehensive performance of SCO_2 in the corrugated tube is better than that in the straight tube. Compared with the straight tube, the stronger secondary flow of the corrugated tube enhances the synergy between local velocity and temperature gradient, thus the heat transfer of SCO_2 in the corrugated tube is enhanced.

References

- [1] Jiang P X, Zhang F Z, Xu R N. Thermodynamic analysis of a solar-enhanced geothermal hybrid power plant using CO_2 as working fluid. *Applied Thermal Engineering*, 2017, 116, 463-472.
- [2] Luu M T, Milani D, McNaughton R, Abbas A. Analysis for flexible operation of supercritical CO_2 Brayton cycle integrated with solar thermal systems. *Energy*, 2017, 124, 752-771.
- [3] Cheng K Y, Zhou J Z, Huai X L, et al. Experimental exergy analysis of a printed circuit heat exchanger for supercritical carbon dioxide Brayton cycles. *Applied Thermal Engineering*, 2021, 192, 116882.
- [4] Liu Z B, He Y L, Yang Y F, et al. Experimental study on heat transfer and pressure drop of supercritical CO_2 cooled in a large tube. *Applied Thermal Engineering*, 2014, 70(1): 307-315.
- [5] Jiang P X, Zhang Y, Shi R F. Experimental and numerical investigation of convection heat transfer of CO_2 at supercritical pressures in a vertical mini-tube. *International Journal of Heat and Mass Transfer*, 2008, 51(11-12): 3052-3056.
- [6] Xu R N, Luo F, Jiang P X. Experimental research on the turbulent convection heat transfer of supercritical pressure CO_2 in a serpentine vertical mini tube. *International Journal of Heat and Mass Transfer*, 2015, 91:552-561.
- [7] Zhu B G, Xu L, Wu X M, et al. Supercritical "boiling" number, a new parameter to distinguish two regimes of carbon dioxide heat transfer in tubes. *International Journal of Thermal Sciences*, 2019, 136:254-266.
- [8] Liu X X, Xu X X, Jiao Y Z, et al. Flow structure with mixed turbulent flow of supercritical CO_2 heated in helically coiled tube. *Applied Thermal Engineering*, 2021, 189, 116684.
- [9] Liu Z B, He Y L, Wang K, et al. Effect of cross section shape of solar collector tube on supercritical CO_2 flow and heat transfer in tube. *Journal of Engineering Thermophysics*, 2018, 39(10): 2235-2243
- [10] Liu Z B, Fei J Y, Yang Y F, et al. Effect of pipe diameter on flow and heat transfer in supercritical CO_2 pipe. *Journal of Engineering Thermophysics*, 2016, 37(2): 357-360.
- [11] Liu X X, Shan H, Zhang S J, et al. Comparative study on heat transfer characteristics of supercritical CO_2 in vertical straight tube and spiral tube. *Journal of Engineering Thermophysics*, 2020, 41(1): 55-60.
- [12] Chika E, Shahid A K, Kwun T L, et al. Numerical study on the heat transfer deterioration and its mitigations for supercritical CO_2 flowing in a horizontal miniature tube. *Annals of Nuclear Energy*, 2021, 151, 107982.
- [13] Yan C S, Xu J L. Numerical analysis of flow and heat transfer

- of supercritical pressure CO₂ in horizontal circular tube. *Journal of Physics*, 2020, 69(4): 044401.
- [14] Wen Q L, Gu H Y. Numerical simulation of heat transfer deterioration phenomenon in supercritical water through vertical tube. *Annals of Nuclear Energy*, 2010, 37(10):1272-1280.
- [15] Liu L, Xiao Z, Yan Z, et al. Heat transfer deterioration to supercritical water in circular tube and annular channel. *Nuclear Engineering and Design*, 2013, 255, 97-104.
- [16] Li Z, Wu Y, Tang G, et al. Comparison between heat transfer to supercritical water in a smooth tube and in an internally ribbed tube. *International Journal of Heat and Mass Transfer*, 2015, 84:529-541.
- [17] Kays W M, Crawford M E, *Convective Heat and Mass Transfer*, McGraw-Hill Inc., New York, 1993.
- [18] Kays W M. Turbulent Prandtl number. *Asme Transactions Journal of Heat Transfer*, 1994, 116(2):284-295.
- [19] Tang G, Shi H, Wu Y, et al. A variable turbulent Prandtl number model for simulating supercritical pressure CO₂ heat transfer. *International Journal of Heat and Mass Transfer*, 2016, 102:1082-1092.
- [20] Weinberg R S, *Experimental and Theoretical Study of Buoyancy Effects in Forced Convection to Supercritical Pressure Carbon Dioxide*, University of Manchester, 1972.